Density Functional Study of Absorption and Resonance Raman Spectra of Pyromellitic Diahydride (PMDA) Anion

T. Andruniow and M. Pawlikowski*

Department of Theoretical Chemistry, Faculty of Chemistry, Jagiellonian University, 30-060 Krakow, Ingardena 3, Poland

M. Z. Zgierski

Steacie Institute for Molecular Sciences, National Research Council of Canada, K1A OR6 Ottawa, Canada

Received: July 15, 1999; In Final Form: November 10, 1999

The electronic structure of the low-energy states of pyromellitic diahydride (PMDA) anion is investigated in terms of density functional theory (DFT). The studies are carried out with a use of the local spin density VWN (Vosco−Wilk−Nusair) and the nonlocal spin density BP (Becke−Perdew) models. To explore the role of the diffuse functions located on carbon and oxygene atoms, the B3LYP method was also employed with 6-31+G* and 6-31G* basis sets. At this level of approximation, the Franck−Condon (FC) parameters were evaluated for the nine totally symmetric modes of PMDA anion in its low-energy dipole-allowed 1^2B_{3g} and 1^2B_{1g} states. These parameters are then employed to reconstruct and discuss the vibrational structure of the experimental absorption and RR spectra measured in the region corresponding to the low-energy $1^2A_u \rightarrow 1^2B_{3g}$ transition. It is shown that a weak mixing of the CC stretching modes upon excitation to the 1^2B_{3g} state and an inhomogeneous broadening of vibronic transitions have a marked effect on the absorption and resonance Raman spectra.

1. Introduction

It is well-known that the cations and anions can be easily studied with the use of the resonance Raman (RR) technique[1−5] applied to gain information not only about the ground but also about the excited states of small and large radicals.[6−15] The absorption spectra of these species show more or less resolved vibrational structures, predominately due to activity of the totally symmetric modes. Accordingly, the resonance Raman spectra of most radicals are dominated by fundamentals, overtones, and combination bands of the totally symmetric vibrations. The intensity distributions of these Raman bands are due to the Franck−Condon (FC) effect well-known from the theory of electronic emission and absorption spectroscopy.

The theory of resonance Raman spectroscopy is well developed and allows one to extract the desired information from the available experimental data.[4,16−23] In particular, an analysis of the FC effects in the excited states of the molecules becomes straightforward when the ground and the excited state(s) geometries are known from sufficiently accurate quantum chemical calculations. With the help of the semiempirical[24,25] or/and ab initio methods,[21,25−27] such calculations can be readily done even for large cationic species. In this respect, the anionic species are much more challenging because ab initio treatments usually require very extensive basis sets in order to describe properly the electron density in the valence states. This is especially true for the larger organic anions that contain "heavy" atoms such as oxygen and/or nitrogen. From our experiences when studying the naphthalene anion,[28] we learned that the MCSCF[29] or CASSCF[30,31] methods may offer one of the best methodologies to deal with the anionic species in their excited electronic states. Nevertheless, certain problems remain. For instance, how large should the MCSCF active orbital space be to describe the subtle changes of the geometry manifested via the FC effects in the excited states of anions. Therefore, although the ab initio MCSCF is certainly the most sophisticated on the formal base, it would be interesting to test how formally less refined but very practical quantum chemical methods might be useful to interpret experimental data available for the relatively large organic anions. The main goal of this paper is to test the density functional theory (DFT) as a tool to explore optical properties of anion radicals in their ground and excited states. For this purpose, the pyromellitic diahydride (PMDA) anion is taken as an important and illustrative example.

We are going to discuss in some detail the FC effects in low-energy excited electronic states of the pyromellitic diahydride (PMDA) anion. The absorption spectrum of that radical measured in the range 14000−30000 cm^{-1} is quite simple and shows only three dipole-allowed electronic transitions.[32] Of these three transitions, the lowest energy dipole-allowed $1^2A_u \rightarrow 1^2B_{3g}$ transition at ca. 15000 cm^{-1} has a relatively simple vibrational structure due to the activity of the totally symmetric modes. Experiment has shown that only four of the nine totally symmetric vibrations are significantly enhanced in the Raman spectra when exciting the PMDA anion in the region corresponding to the 1^2B_{3g} state.[6] These spectra are subject to our analysis performed in terms of the DFT method applied on different levels of approximation, namely, the local spin density VWN (Vosco−Wilk−Nusair)[33] and the nonlocal spin density BP (Becke−Perdew)[34] approximations. The results of Becke's three-parameter hybrid method with Lee−Yang−Parr correlation functional (B3LYP)[35,36] are also presented. In the analysis of the RR spectra, we neglect the vibronic coupling effects and we treat the vibrations as the displaced harmonic oscillators. The potentially important effects such as normal coordinates

10.1021/jp992411b CCC: $19.00
Published on Web 01/06/2000

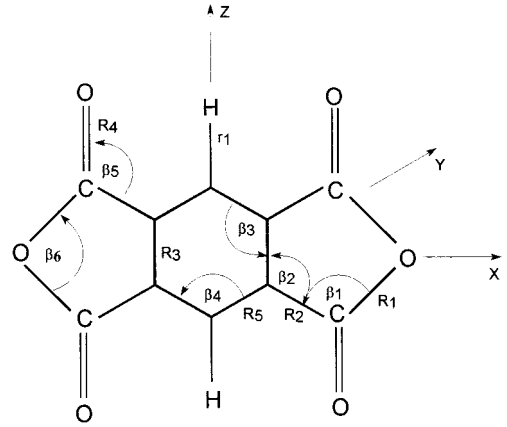

Figure 1. Geometric structure of the PMDA anion. The values of the bond lengths and bond angles in the ground (1^2A_u) and two excited (1^2B_{2u}, 1^2B_{3g}) states are given in Table 1.

TABLE 1: The Optimized Geometry (Å, deg) Achieved from B3LYP/6-31+G* and B3LYP/6-31G* Computations[a]

coordinate	1^2A_u	1^2B_{2u}	$^2B_{3g}$
R_1	1.4099 (1.4097)	1.4094 (1.4092)	1.4002 (1.4002)
R_2	1.4528 (1.4524)	1.4675 (1.4667)	1.4708 (1.4709)
R_3	1.4373 (1.4363)	1.3932 (1.3917)	1.4104 (1.4091)
R_4	1.2172 (1.2151)	1.2112 (1.2100)	1.2239 (1.2225)
R_5	1.3935 (1.3922)	1.4201 (1.4191)	1.4021 (1.4010)
r_1	1.0865 (1.0863)	1.0822 (1.0816)	1.0848 (1.0843)
β_1	106.90 (106.91)	108.43 (108.44)	106.71 (106.67)
β_2	107.70 (107.71)	107.59 (107.60)	107.77 (107.81)
β_3	121.86 (121.81)	123.20 (123.18)	122.25 (122.19)
β_4	116.29 (116.38)	113.61 (113.64)	115.49 (115.62)
β_5	132.31 (132.16)	130.97 (130.91)	130.97 (130.88)
β_6	110.79 (110.75)	107.97 (107.91)	111.03 (111.04)

[a] The results of B3LYP/6-31G* are given in parentheses.

rotation[37,38] in the 1^2B_{3g} and 1^2B_{1g} states are also briefly discussed.

There is a wide class of the aromatic molecules which are capable of forming donor−acceptor crystals in which acid anhydrides play a role of electron acceptors.[39] The optical properties of these crystals are, to great extent, dependent on the electronic and vibrational structures of the acceptor and the donor alone. The anthracene−PMDA and the pyrene−PMDA crystals can serve here as the apparent and the well-known examples.[39−41] The theoretical treatment of the CT states in such crystals[42−44] requires knowledge of localized electronic excitation energies and FC factors for electronic transitions in a donor and in an acceptor. One of the purposes of this paper is to provide a simple and practical calculation base for the evaluation of these parameters in a quantum chemical way.

2. Methods and Computational Details

The geometrical structure of the PMDA anion and the orientation of the Cartesian axes applied in the computations are given in Figure 1. The PMDA anion is flat so that the Cartesian components *x*, *y*, and *z* transform, respectively, as B_{3u}, B_{2u}, and B_{1u} representations of the D_{2h} point group. It implies that the following selection rules: $A_u \rightarrow B_{3g}$ (*x* polarization), $A_u \rightarrow B_{2g}$ (*y* polarization), and $A_u \rightarrow B_{1g}$ (*z* polarization) must apply for the dipole-allowed transitions.

For the ground state (1^2A_u) and the lowest energy 1^2B_{2u} and 1^2B_{3g} states, the values of the bond lengths r_i and R_i and bond angles β_i (Figure 1) are collected in Table 1. They were obtained by the geometry optimization procedures available from GAUSSIAN 94 program package.[45] To get the entries of Table 1 we applied the B3LYP method, which is a combination of Becke's three-parameter hybrid exchange functional with the Lee−Yang−Parr[35] correlation functional. One of the exchange functionals is the exact Hartree−Fock exchange functional based on the Kohn−Sham orbitals. Two basis sets, 6-31+G* and 6-31G*, were chosen to test an influence of the diffuse functions localized on the carbon and oxygen atoms on the FC parameters and frequencies of vibrational modes. The ground state frequencies of the PMDA anion and their symmetry assignments as obtained from the B3LYP/6-31+G* and B3LYP/6-31G* treatments are given in Table 2. As follows from Table 2, the results of both methods differ only slightly so that the effect of diffuse functions is not critical for the ground state (1^2A_u) calculations. We checked that the same applies at least for the 1^2B_{3g} state of PMDA anion.

To get better insight into the quality of the DFT results, we also made the computations within the local spin density VWN (Vosco−Wilk−Nusair) and the nonlocal spin density BP (Becke−Perdew) approximations.[46] Both methods were employed with the double numerical functions augmented by polarization functions (DNP). These functions are commonly viewed to be equivalent to the Pople 6-31G*-type basis set.[46] In all computations, the inner core electrons (1s) of the carbon and oxygen atoms were frozen.

For the low-energy states of the PMDA anion, the adiabatic transition energies and the corresponding transition dipole moments found within four approximations are summed up in Table 3. As follows from Table 3, the DFT results are very consistent in the series B3LYP/6-31+G*, B3LYP/6-31G*, VWN/DNP, and BP/DNP. However, it should be noted that the B3LYP treatments are much more time-consuming than VWN/DNP and BP/DNP treatments. Typically, both B3LYPs take 100 or 1000 more seconds of processor time than the VWN/DNP and BP/DNP treatments do in order to accomplish a task on the same computer.

In Table 4, we give a sample of the FC parameters computed for the two most intense $1^2A_u \rightarrow 1^2B_{3g}$ and $1^2A_u \rightarrow 1^2B_{1g}$ transitions discussed in detail in the subsequent sections. The Franck−Condon (dimensionless) parameters $B_{x,i}$ of the *i*th vibration in the X electronic state were calculated from the expression[21,24]

$$B_{x,i} = \mathbf{S}_i^{\mathrm{T}} \cdot \mathbf{F}(\mathrm{X,G}) \left(\frac{\hbar}{\mu_i \omega_i} \right)^{-1} \qquad (1)$$

where $\mathbf{S}_i$ is a column vector containing the Cartesian nuclear displacements in Q_i normal mode with the frequency ω_i and reduced mass μ_i. $\mathbf{F}$(X,G) is the column vector containing the differences of the nuclear position vectors in the excited X state and the ground G state equilibrium configurations. In the calculations leading to the entries in Table 4, the vibrational (normal) coordinates were taken to be the same in the ground and the excited states. It amounts to an assumption that neither the vibrational frequency changes nor the Dushinsky rotation[37,38] are large in the 1^2B_{3g} and 1^2B_{1g} states. The consequences of this assumption are discussed in the subsequent section.

3. PMDA Anion Absorption

In the visible and near UV range 14000−30000 cm^{-1}, the absorption spectrum of the PMDA anion[32] shows two intense bands. In this energy range, the DFT calculations (Table 3) predict three dipole-allowed $1^2A_u \rightarrow 1^2B_{3g}$, $1^2A_u \rightarrow 1^2B_{2g}$, and $1^2A_u \rightarrow 1^2B_{1g}$ transitions. The $1^2A_u \rightarrow 1^2B_{3g}$ and $1^2A_u \rightarrow 1^2B_{1g}$ transitions are in-plane polarized being $\pi-\pi^*$ in character. The

TABLE 2: Frequencies (cm^{-1}) Obtained from B3LYP/6-31+G* and B3LYP/6-31G* (in Parentheses)

	a_g	b_{1g}	b_{2g}	b_{3g}	b_{1u}	b_{2u}	b_{3u}	a_u
ν_1	3212 (3210)	734 (733)	1752 (1784)	937 (944)	3211 (3210)	939 (932)	1768 (1807)	730 (735)
ν_2	1840 (1869)	260 (261)	1502 (1509)	723 (748)	1769 (1800)	720 (720)	1483 (1492)	414 (453)
ν_3	1585 (1593)	182 (186)	1225 (1220)	576 (624)	1499 (1505)	413 (420)	1404 (1407)	71 (73)
ν_4	1331 (1342)		1049 (1055)	201 (207)	1193 (1198)	190 (192)	1242 (1254)	
ν_5	1121 (1132)		824 (827)		883 (890)	92 (93)	1062 (1062)	
ν_6	753 (755)		706 (707)		768 (772)		765 (766)	
ν_7	639 (641)		546 (547)		583 (585)		611 (614)	
ν_8	481 (484)		259 (255)		171 (170)		379 (380)	
ν_9	279 (279)							

TABLE 3: Transition Energies (eV) and Assignments for Four Low-Energy States of PMDA Anion[a]

	B3LYP 6-31+G*	B3LYP 6-31G*	B-P DNP	VWN DNP	description
$D_1-1^2B_{2u}$	0.991 (0.00)	1.010 (0.00)	0.898 (0.00)	0.930 (0.00)	$2a_u \rightarrow 4b_{2u}$
$D_2-1^2B_{3g}$	1.722 (3.53)	1.774 (3.29)	1.417 (3.77)	1.433 (3.72)	$2a_u \rightarrow 3b_{3g}$
$D_3-1^2B_{2g}$			2.611 (0.07)	2.637 (0.08)	$6b_{2g} \rightarrow 2a_u$
$D_4-1^2B_{1g}$		2.976 (−)	2.903 (1.87)	3.003 (1.96)	$3b_{1g} \rightarrow 2a_u$

[a] The transition dipole moments (D) are given in parentheses.

TABLE 4: Frequencies $\nu_{0,i}$ (cm^{-1}) and FC Parameters for a Few Low-Energy States of PMDA Anion Obtained from B3LYP/6-31+G*, B3LYP/6-31G*, VWN/DNP, and BP/DNP Methods

B3LYP/6-31+G*		B3LYP/6-31G*			VWN/DNP			BP/DNP		
$\nu_{0,i}$	1^2B_{3g}	$\nu_{0,i}$	1^2B_{3g}	1^2B_{1g}	$\nu_{0,i}$	1^2B_{3g}	1^2B_{1g}	$\nu_{0,i}$	1^2B_{3g}	1^2B_{1g}
3212	0.04	3210	0.05	0.01	3141	0.03	0.03	3126	0.03	0.01
1840	0.07	1869	0.03	0.32	1831	0.04	0.43	1700	0.05	0.39
1585 [1548][a]	0.32	1593	0.32	1.01	1590	0.27	0.92	1494	0.36	1.04
1331 [1316]	0.74	1342	0.77	1.08	1345	0.66	1.02	1223	0.70	1.05
1121 [1110]	0.36	1132	0.31	0.51	1128	0.35	0.49	1024	0.43	0.46
753	0.02	755	0.00	1.09	742	0.11	0.96	712	0.02	1.04
639	0.19	641	0.14	1.37	626	0.15	1.20	583	0.20	1.42
481 [480]	0.58	484	0.59	0.52	486	0.48	0.42	479	0.41	0.22
279	0.03	279	0.02	0.11	283	0.09	0.25	246	0.20	0.30

[a] Experimental data from ref 6. Description of the totally symmetric modes: ν_1 (C−H stretch), ν_2 (C═O stretch), ν_3, ν_4 (C−C stretch), ν_5 (C−C + C═O stretch), ν_6 (C−C stretch + CCC central ring deformation), ν_7 (C−C═O deformation), ν_8 (C−C═O deformation + CCC central ring deformation), ν_9 (C−C−C central ring deformation + C═O wagging).

third extremally weak $1^2A_u \rightarrow 1^2B_{2g}$ transition is polarized perpendicular to the plane of the PMDA molecule and is due to $\pi-\sigma^*$ single electron promotion. The resulting absorption spectrum is thus very simple and resembles that obtained earlier from the Longuet−Higgins and Pople semiempirical method.[32] There is also a fourth $1^2A_u \rightarrow 1^2B_{2u}$ transition located by our computation at ca. 7650 cm^{-1} above the ground state. This transition is forbidden and absent from the measured absorption of the PMDA. The virtual absence of this transition from the measured absorption may suggest that the vibronic couplings via the b_{1u} and b_{3u} modes in the electronic manifolds of 1^2B_{2u}, 1^2B_{3g}, and 1^2B_{1g} states should be weak or very weak.

Figure 2 presents the experimental (top) and the theoretical absorption spectra calculated from the B3LYP/6-31G*, VWN/DNP, and BP/DNP methods in the regions corresponding to the $1^2A_u \rightarrow 1^2B_{3g}$ and $1^2A_u \rightarrow 1^2B_{1g}$ transitions. All theoretical spectra were obtained as superpositions of the Lorentzian curves with the line widths $\Gamma(1^2B_{3g}) = 100$ cm^{-1} and $\Gamma(1^2B_{1g}) = 250$ cm^{-1}. Since the dipole-allowed $1^2A_u \rightarrow 1^2B_{2g}$ transition is about 3.4×10^{-4} times weaker than remaining two, its additive contribution to the absorption at 25000−30000 cm^{-1} could be neglected in the absence of any vibronic coupling between the 1^2B_{2g} and 1^2B_{1g} states via vibrational modes of the b_{3g} symmetry. To simplify a comparison between the intensities of different spectra, the energies of 0−0 transitions were synchronized to those known from the experiment. So, except for these energy shifts made to improve presentation, no other scaling was applied to simulate the absorption depicted in Figure 2.

From Figure 2, we can see that the agreement between the theory and experiment is quite reasonable even if certain discrepancies occur and claim for model refinements. For the $1^2A_u \rightarrow 1^2B_{1g}$ band, the three DFT methods lead to similar intensity distributions that refect the strong FC effects in the 1^2B_{1g} state. Two peaks seen on the left wing of the experimental absorption at 25510 and 26178 cm^{-1} can be ascribed to the fundamental and to the overtone of the $\nu_7 = 641$ cm^{-1} vibration, respectively.[32] This observation agrees with the VWN/DNP, BP/DNP, and B3LYP/6-31G* results (Table 4) and suggests that the ν_7 mode is one of the most activite among the low-frequency a_g symmetry modes. Since the FC effects are strong in the 1^2B_{1g} state, the remaining peaks in the $1^2A_u \rightarrow 1^2B_{1g}$ band appear as superpositions of multimode contributions. On the other hand, the band-shape of the low-energy $1^2A_u \rightarrow 1^2B_{3g}$ transition reflects the weak FC effects in the 1^2B_{3g} state. From Figure 2, one can see that the low-energy band has relatively well-resolved vibrational structure dominated by the single-mode transitions. These can be easily identifed as the vibrations with the ground state (B3LYP/6-31G*) frequencies $\nu_8 = 484$ cm^{-1}, $\nu_5 = 1132$ cm^{-1}, $\nu_4 = 1342$ cm^{-1}, and $\nu_3 = 1593$ cm^{-1}. It follows that for the visible $1^2A_u \rightarrow 1^2B_{3g}$ band, the VWN/DNP, BP/DNP, and B3LYP/6-31G* methods yield a very similar intensity pattern which closely resembles that one observed in the empirical absorption. However, the agreement between theory and experiment is clearly not perfect, especially for the excitation energy region at 16000−16500 cm^{-1}. Particularly, we can see that the three DFT treatments overestimate FC activity of the $\nu_4 = 1342$

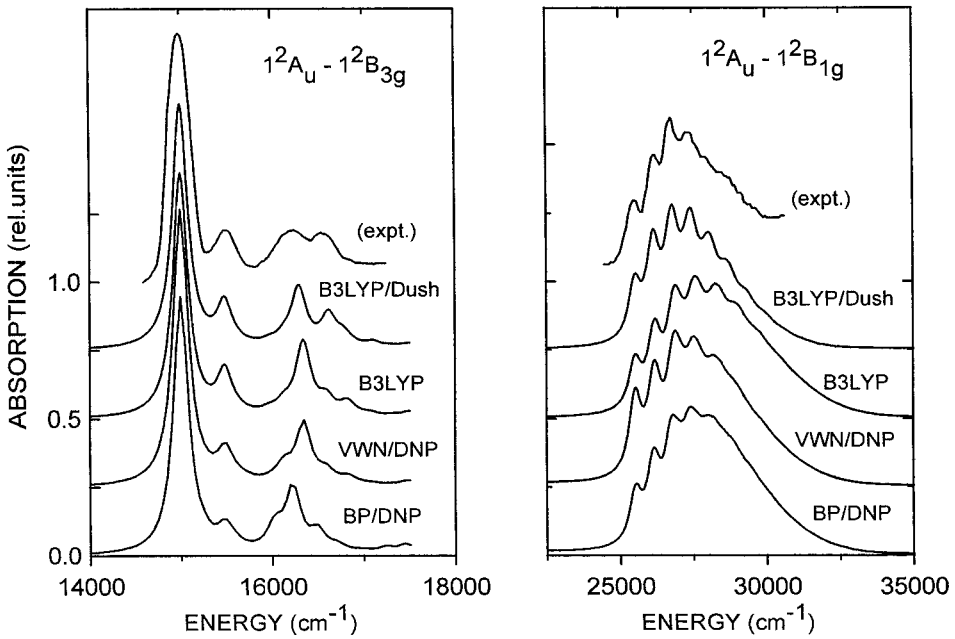

Figure 2. Experimental (top) and the theoretical (bottom) absorption spectra in the regions corresponding to the $1^2A_u \rightarrow 1^2B_{3g}$ and $1^2A_u \rightarrow 1^2B_{1g}$ transitions. The FC parameters used in the calculations are given in Table 4 (BP/DNP, WVN/DNP, and B3LYP/6-31G*) and Table 5 (B3LYP/Dush). The line widths $\Gamma(1^2B_{3g}) = 100$ cm^{-1} and $\Gamma(1^2B_{1g}) = 250$ cm^{-1} were used in the calculations.

TABLE 5: Frequencies (cm^{-1}) of Totally Symmetric Vibrations in the 1^2B_{3g} and 1^2B_{1g} States of PMDA Anion Calculated from the B3LYP/6-31G* Method[a]

$\nu_{0,i}$	ν_{mi} (1^2B_{3g})	ν_{ni} (1^2B_{1g})
3210		3210 (0.01)
1842	1837 (0.14)	1796 (0.42)
1593	1621 (0.49)	1528 (0.50)
1342	1295 (0.69)	1306 (1.03)
1132	1135 (0.24)	1098 (0.50)
755	761 (0.06)	714 (0.91)
641	644 (0.10)	615 (1.52)
484	483 (0.59)	473 (0.55)
279	271 (0.02)	277 (0.01)

[a] The FC parameters frenormalized due to Dushinsky rotation according to the model of ref 48 are given in parenthesesThis paper needs a title running head (TRH).

cm^{-1} vibration and underestimate the activities of $\nu_5 = 1132$ cm^{-1} and $\nu_3 = 1593$ cm^{-1} vibrations in the low-energy $1^2A_u \rightarrow 1^2B_{3g}$ band. Since the calculated absorption spectra are so consistent for such different DFT methods, we surmise that the drawbacks observed near 16500 cm^{-1} may be in large part due to limitations of the vibronic model rather than due to low accuracy of the DFT computations. Specifically, it is conceivable that the inclusion of the mode-mixing (Dushinsky) effects in the ν_3, ν_4, and ν_5 vibrations could improve the agreement between theory and experiment in the debatable region.[47]

To check this possibility, we performed appropriate calculations based on the model already known in the literature.[48] The ground and the excited state frequencies and the vibrational coordinates were determined from the B3LYP/6-31G* method. Then, they were used to find the FC parameters renormalized to take into account the mode mixing in the excited state(s). These parameters together with the excited state vibrational frequencies are collected in Table 5 for the 1^2B_{3g} and 1^2B_{1g} states of the PMDA anion. They lead to the absorption spectra labeled as B3LYP/Dush in Figure 2.

Comparing the numbers in Table 5 to those given in Table 4, we can see that the B3LYP/6-31G* FC parameters do not differ drastically from their renormalized B3LYP/Dush counterparts. It means that the mode-mixing effects are weak in both 1^2B_{3g} and 1^2B_{1g} states. Nevertheless, it follows from Figure 2 that even a weak Dushinsky effect causes a splitting of the band at 16500 cm^{-1} and tends to suppress the intensity of the $\nu_4 = 1342$ cm^{-1} mode and increase the activity of the $\nu_3 = 1593$ cm^{-1} vibration. Such a behavior is required to establish the correct intensity distribution in the theoretical absorption of the $1^2A_u \rightarrow 1^2B_{3g}$ band near 16500m^{-1}. Since the intensity distributions of the $1^2A_u \rightarrow 1^2B_{1g}$ band obtained from B3LYB/Dush and B3LYP/6-31G* schemes do not differ much, apparently weak Dushinsky effects in the 1^2B_{1g} state of PMDA anion have a moderate influence on the band shape in the debatable absorption region.

To close this section, we have to comment on the $1^2A_u \rightarrow 1^2B_{2g}$ transition, located through the VWN/DNP and BP/DNP approaches about 0.29−0.34 eV lower in energy than the intense $1^2A_u \rightarrow 1^2B_{1g}$ transition (Table 3). Thus far, the presence of that extremally weak transition was not experimentally evidenced, and we believe that the $1^2A_u \rightarrow 1^2B_{2g}$ transition is hidden in the intense and broad $1^2A_u \rightarrow 1^2B_{1g}$ band. It should be noted that the $1^2A_u \rightarrow 1^2B_{2g}$ and $1^2A_u \rightarrow 1^2B_{1g}$ transitions are of different polarizations. Therefore, the experimental techniques naturally oriented to study the polarization effects could be helpful to verify the localization of the 1^2B_{2g} state and to answer the questions about possible vibronic couplings between 1^2B_{2g} and 1^2B_{1g} states. Resonance Raman spectroscopy is one of such techniques allowing study of the polarization effects through depolarization dispersion measurements. To the best of our knowledge, empirical data of that kind have not been reported as yet in the region corresponding to the $1^2A_u \rightarrow 1^2B_{1g}$ transition. However, the RR spectra were already reported for a few laser excitation energies corresponding to the low-energy $1^2A_u \rightarrow 1^2B_{3g}$ transition.[6] So, in the next section, we take an advantage of these spectra to verify the results of DFT calculations presented in this paper.

4. PMDA Anion Resonance Raman Spectra

While the 1^2B_{2g} and 1^2B_{1g} states may be subject to vibronic coupling effects, the experiment and the DFT calculations are

consistent in the conclusion that the 1^2B_{3g} state is well separated on the energy scale from other excited electronic states of the PMDA anion. Therefore, the model formulated earlier[4,21] can be applied readily for purposes of this section. To this end, let the energy of the laser light, Ω, be in resonance with the *x*-polarized $1^2A_u \rightarrow 1^2B_{3g}$ transition and let the transition dipole matrix element $\langle A_u|D_x|B_{3g}\rangle$ depend weakly on the vibrational coordinates. At this level, the scattering tensor has only one nonvanishing element which can be calculated from[4,21]

$$\alpha_{xx}^{0\rightarrow k} = |\langle A_u|D_x|B_{3g}\rangle|^2 \sum_{\nu_1}\sum_{\nu_i}\sum_{\nu_N} \frac{(\Lambda_k(A_u)|\Lambda_v(B_{3g}))(\Lambda_v(B_{3g})|\Lambda_o(A_u))}{E_o + \epsilon_v - \Omega - i\Gamma_v} \quad (2)$$

where E_0 ($=E(B_{3g}) - E(A_u)$) is the adiabatic excitation energy and ϵ_v is the vibrational energy calculated from

$$\epsilon_v = \sum_{i=1}^{N} \hbar\omega_{o,i} v_i \quad (3)$$

In eq 2, $\Lambda_k(A_u)$ and $\Lambda_v(B_{3g})$ are the vibrational functions of the 1^2A_u and 1^2B_{3g} electronic states. The vectors $\mathbf{k} = (k_1, k_i, k_N)$ and $\mathbf{v} = (v_1, v_i, v_N)$ denote the sets of vibrational quantum numbers in the ground and the excited state, respectively. The vibrational overlap integrals $(\Lambda_k(A_u)|\Lambda_v(B_{3g}))$ and $(\Lambda_v(B_{3g})|\Lambda_o(A_u))$ can be determined from the well-known recursion formulas given elsewhere.[23] In eq 2, Γ_v is the line width resulting from all homogeneous (radiative and nonradiative) processes. In an attempt to take also the inhomogeneous broadening[49,50] into account, we assumed that the excitation energy, E_0, is "diffused" due to different local environment of the different molecules in the sample. In a reasonable approximation, the effect can be described by the Lorentzian-type probability distribution function[4,50]

$$p(E,E_o) = \frac{\Delta}{\pi}\frac{1}{(E - E_o)^2 + \Delta^2} \quad (4)$$

so that the Raman intensities should be evaluated from

$$I(0\rightarrow k) = \Omega(\Omega - \hbar\omega_{0,k})^3 I_0 \int_0^\infty p(E,E_o)\overline{|\alpha_{xx}^{0\rightarrow k}|^2}\, dE \quad (5)$$

where I_o and $I(0\rightarrow k)$ are the intensities of the incident and scattered beams, respectively, and the bar denotes an orientational average. With the assumption that the homogeneous line widths are the same for all vibronic levels ($\Gamma_v = \Gamma$), Γ and Δ remain as the only adjustable model parameters.

The effect of homogeneous and inhomogeneous broadenings on the two selected Raman bands is illustrated in Figure 3. The two excitation profiles $\Theta(2\nu_8)$ and $\Theta(\nu_4)$ shown in Figure 3 were calculated for $\Gamma = 95$ cm^{-1} and $\Delta = 5$ cm^{-1} (top) and $\Gamma = 5$ cm^{-1} and $\Delta = 95$ cm^{-1} (bottom) and for the B3LYP/Dush input parameters listed in Table 5. Because the homogeneous effect is governed by the Lorentzian distribution function (4), the absorption spectrum is a superposition of the Lorentzians with the bandwidths $\Gamma + \Delta = 100$ cm^{-1}. Therefore, both sets of the excitation profiles presented in Figure 3 correspond to the B3LYP/Dush absorption spectrum given in Figure 2.

At the first glance, the effect of inhomogeneity on the Raman intensities seems to be of minor importance, but a closer inspection of the $\Theta(2\nu_8)$ and $\Theta(\nu_4)$ curves reveals that inhomogenoues effect may reduce the Raman intensity of the ν_4 fundamental almost twice when Ω falls between two maxima of the $\Theta(\nu_4)$ profile. Such a behavior, which reflects the interference phenomena,[23] will also occur for the two ν_5 and ν_4 most FC-active fundamental bands. As a result, the RR spectrum at $\Omega = 15504$ cm^{-1} should be dominated by the overtones and combination bands while the fundamentals are expected to be weak. This is in fact observed in Figure 4, where we compare the experimental (curves) and theoretical (sticks) RR spectra reported for two laser excitation energies:[6] $\Omega = 15152$ cm^{-1} and $\Omega = 15504$ cm^{-1}. For $\Omega = 15152$ cm^{-1}, the laser wavelength coincides roughly with the transition into the blue

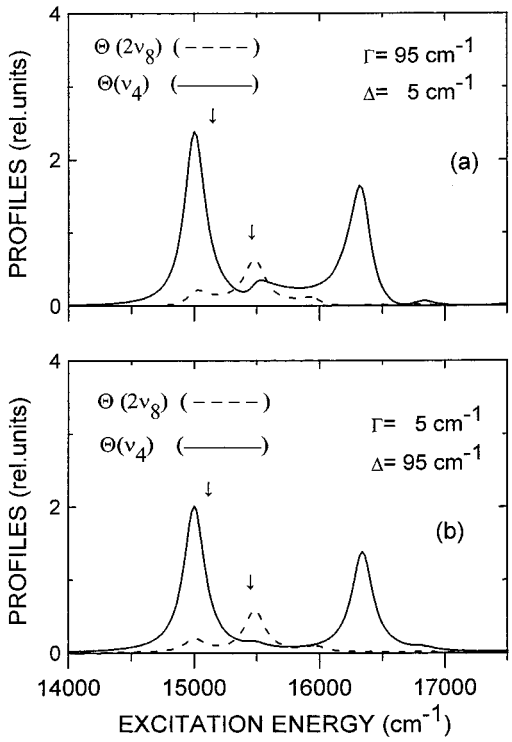

Figure 3. Excitation profiles calculated for the ν_4 fundamental (—) and $2\nu_8$ overtone (- - -) over the region corresponding to the $1^2A_u \rightarrow 1^2B_{3g}$ band. The FC parameters are the same as B3LYP/Dush absorption in Figure 2. The homogeneous and inhomogeneous broadenings are (a) $\Gamma = 95$ cm^{-1}, $\Delta = 5$ cm^{-1} and (b) $\Gamma = 5$ cm^{-1}, $\Delta = 95$ cm^{-1}. The arrows indicate the excitation energies $\Omega = 15152$ cm^{-1} and $\Omega = 15504$ cm^{-1}.

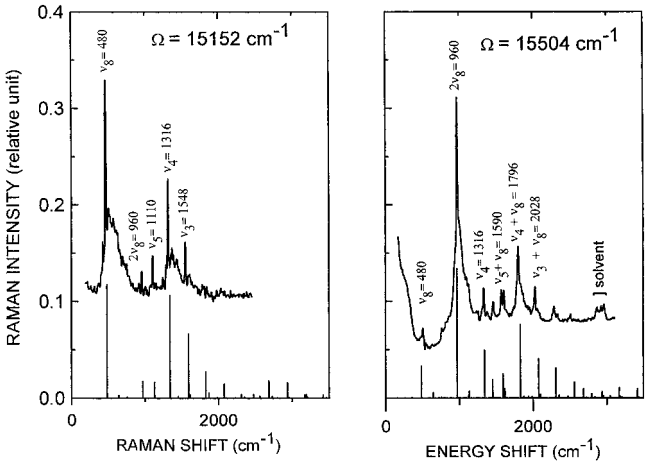

Figure 4. Calculated (stick) and theoretical RR spectra at $\Omega = 15\,152$ cm^{-1} and $\Omega = 15\,504$ cm^{-1}. The FC parameters are the same as those for the B3LYP/Dush absorption in Figure 2. The homogeneous and inhomogeneous broadening parameters are $\Gamma = 5$ cm^{-1} and $\Delta = 95$ cm^{-1}.

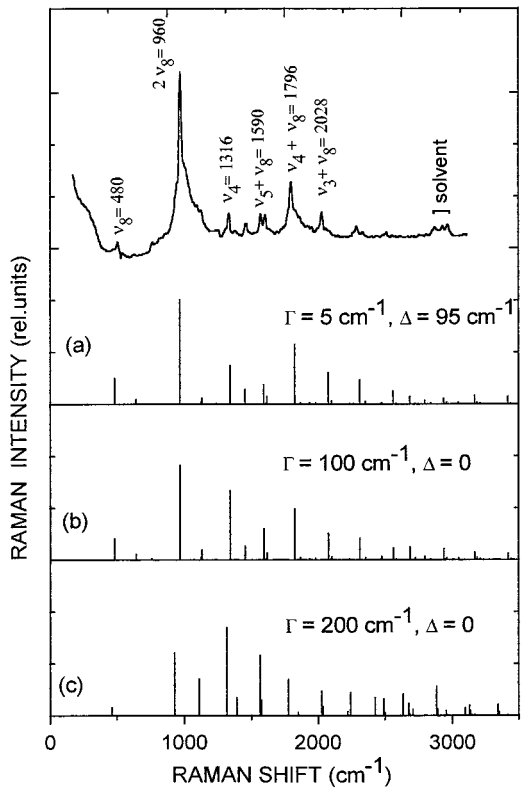

Figure 5. Comparison between the calculated and the empirical RR spectra at $\Omega = 15504$ cm^{-1}. For panels a and b, the FC parameters as Figure 4. The stick spectrum in the panel c was achieved with FC parameters $B_{463} = 0.833$, $B_{1110} = 0.512$, $B_{1316} = 0.836$, and $B_{1564} = 0.717$ estimated in ref 6.

end of the origin of the 1^2B_{3g} manifold, and, accordingly for small displacement parameters, the RR spectrum is dominated by the fundamental bands. On the other hand, for $\Omega = 15504$ cm^{-1}, the laser wavelength coincides roughly with the excitation into the fundamental of the ν_8 mode, and accordingly, the spectrum is dominated by the overtone of this mode and by the combination bands of the ν_8 and other FC-active modes (ν_3, ν_4, and ν_5). In our simulation, we have used displacement parameters and frequencies obtained in B3LYP/Dush scheme. We wish to note that displacement parameters and frequencies obtained from VWN/DNP and BP/DNP calculations also give a good, albeit somewhat inferior argeement with the experimental data. The values of homogeneous and inhomogeneous broadenings $\Delta = 95$ cm^{-1} and $\Gamma = 5$ cm^{-1} were used in the calculations leading to the Raman spectra in Figure 4.

A look at Figure 4 shows that the agreement between the theory and experiment is in general satisfactory. The Raman spectrum at $\Omega = 15152$ cm^{-1} is essentially dominated by the fundamental transitions, and the only very weak Raman feature at 960 cm^{-1} can be identified as the overtone of the ν_8 mode, in agreement with the experiment. However, a closer inspection of the RR spectrum at $\Omega = 15152$ cm^{-1} shows that the calculated intensity of the ν_4 fundamental is slightly underestimated comparing to its experimental counterpart. The same occurs for the first overtone of the ν_8 vibration as seen in the RR spectrum at $\Omega = 15504$ cm^{-1}. It is worth noting that these minor differences between the simulated and empirical RR spectra would be much larger if the inhomogeneous effect had been completely neglected. This is seen better from Figure 5 where Raman spectra at $\Omega = 15504$ cm^{-1} obtained for $\Gamma = 5$ cm^{-1} and $\Delta = 95$ cm^{-1} (Figure 5a) and $\Gamma = 100$ cm^{-1} and $\Delta = 0$ (Figure 5b) are compared. Although the calculations leading to parts a and b of Figure 5 were performed with the same set of FC (B3LYP/Dush) parameters, the intensity distribution in the RR spectrum are quite different, especially for the ν_4 fundamental and $\nu_4 + \nu_8$ combination band. This underscores the sensitivity of RR spectra to different forms of line broadening as it was first pointed out in ref 23.

Finally, we wish to note that the RR spectra discussed in this paper were the subject of theoretical analysis in the original Sheng and Hug paper.[6] Figure 5 presents a comparison between their results and ours. The stick RR spectrum in Figure 5c was calculated within a four-mode approximation with the FC parameters $B_{463} = 0.833$, $B_{1110} = 0.512$, $B_{1316} = 0.836$, and $B_{1564} = 0.717$, as evaluated in the original paper.[6] These FC parameters are much larger than needed to account even qualitatively for the experimental data. Moreover, the RR spectrum reported as Figure 3c in ref 6 should be the same as that shown in Figure 5c of this paper. Because this is not so, there is reason to believe that the fitting procedure employed in the original paper was probably subject to some numerical errors.

5. Conclusion

The structure and the force fields of the ground 1^2A_u and the two excited states 1^2B_{3g} and 1^2B_{1g} of the PMDA anion have been studied with the help of density functional theory methods. It has been shown that, surprisingly, diffuse orbitals have only a minor effect on these properties. The displacement parameters and the Dushinsky matrices for the $1^2A_u \rightarrow 1^2B_{3g}$ and the $1^2A_u \rightarrow 1^2B_{1g}$ have been extracted from the DFT calculations and applied to simulate absorption as well as the resonance Raman spectra obtained within the $1^2A_u \rightarrow 1^2B_{3g}$ absorption band. Good agreement between theory and experiment was obtained without any modifications of the parameters achieved from DFT theory. We have shown that a weak mixing of the CC stretching modes of the anion upon excitation to the 1^2B_{3g} state has a marked effect on the absorption and resonance Raman spectra. Finally, we have demonstrated that the inhomogeneous broadening of vibronic transitions must be included to reproduce the observed resonance Raman spectra.

Acknowledgment. One of us (T.A.) thanks Jagiellonian Computing Center for access to the Silicon Graphics ONYX workstation and Academic Computer Center ("Cyfronet") for the Convex SPP 1600 computer time. The grant from the Polish State Committee for Scientific Research (3T09A 10615) is acknowledged.

References and Notes

(1) Tang, J.; Albrecht, A. C. In *Raman spectroscopy-theory and practice*; Szymanski, H. A., Ed.; Plenum Press: New York, 1970; Volume 2.

(2) Warshel, A. *Annu. Rev. Biophys. Bioeng.* **1977**, *6*, 273.

(3) Champion, P. M.; Albrecht, A. C. *Annu. Rev. Phys. Chem.* **1982**, *33*, 353.

(4) Siebrand, W.; Zgierski, M. Z. In *Excited states*; Lim, E. C., Ed.; Academic Press: New York, 1979; Chapter 1.

(5) Asher, S. A. *Annu. Rev. Phys. Chem.* **1988**, *39*, 537.

(6) Sheng, S. J.; Hug, G. *Chem. Phys. Lett.* **1978**, *57*, 168.

(7) Li, P. C.; Devlin, J. P.; Pohl, H. A. *J. Phys. Chem.* **1972**, *76*, 1026.

(8) Takahashi, C.; Maeda, S. *Chem. Phys. Lett.* **1973**, *22*, 364.

(9) Bazio, R.; Girlando, A.; Pacile, C. *J. Chem. Soc., Faraday Trans.* **1975**, *71*, 1237.

(10) Girlando, A.; Bazio, R.; Pacile, C. *Chem. Phys. Lett.* **1974**, *25*, 403.

(11) Chi, C. K.; Nixon, E. R. *Spectrochim. Acta* **1975**, *A31*, 1739.

(12) Jeanmaire, D. L.; Van Duyne, R. P. *J. Am. Chem. Soc.* **1976**, *98*, 4029; **1976**, *98*, 4034.

(13) Takahashi, C.; Maeda, S. *Chem. Phys. Lett.* **1974**, *24*, 584.

(14) Takahashi, C.; Maeda, S. *Chem. Phys. Lett.* **1974**, *28*, 22.
(15) Mayer, E.; Girling, R. B.; Hester, R. E. *J. Chem. Soc., Chem. Commun.* **1973**, 192.
(16) Pawlikowski, M. *Acta Phys. Pol.* **1983**, *A63*, 547.
(17) Henneker, W. H.; Siebrand, W.; Zgierski, M. Z. *J. Chem. Phys.* **1981**, *74*, 6560.
(18) Zborowski, K.; Pawlikowski, M. *Acta Phys. Pol.* **1995**, *88*, 435.
(19) Sassi, P.; Pawlikowski, M. *Acta Phys. Pol.* **1996**, *90*, 509.
(20) Hoskins, L. C.; Pham, A. X.; Rutt, G. C. *J. Raman Spectrosc.* **1990**, *21*, 543. Hoskins, L. C. *J. Chem. Phys.* **1981**, *74*, 882. Hoskins, L. C. *Spectrochim. Acta* **1986**, *42A*, 169.
(21) Andruniow, T.; Zborowski, K.; Pawlikowski, M. *Chem. Phys. Lett.* **1996**, *259*, 193.
(22) Rush, T., III; Peticolas, W. L. *J. Phys. Chem.* **1995**, *99*, 14647.
(23) Siebrand, W.; Zgierski, M. Z. *J. Chem. Phys.* **1979**, *71*, 3561.
(24) Orlandi, G.; Zerbetto, F.; Zgierski, M. Z. *Chem. Rev.* **1991**, *91*, 867.
(25) Negri, F.; Zgierski, M. Z. *J. Chem. Phys.* **1994**, *100*, 1387.
(26) Andruniow, T.; Pawlikowski, M. *Chem. Phys.* **1998**, *236*, 25.
(27) Andruniow, T.; Pawlikowski, M. *Chem. Phys.* **1998**, *236*, 35.
(28) Andruniow, T.; Pawlikowski, M. *Acta Phys. Pol.* **1998**, *93*, 707.
(29) Ruedenberg, K.; Smidt, M. W.; Gilbert, M. M.; Elbert, S. T. *Chem. Phys.* **1982**, *71*, 41 and references therein.
(30) Andersson, K.; Malmqvist, P. A.; Roos, B. O.; Sadlej, A. J.; Wolinski, K. *J. Phys. Chem.* **1990**, *94*, 5483.
(31) Andersson, K.; Roos, B. O. In *Modern electron structure theory, Multiconfigurational second-order perturbational theory*; Yarkonyl, R., Ed.; World Science: Singapore, 1994; Vol. 1 and references therein.
(32) Shida, T.; Iwata, S.; Imamura, M. *J. Phys. Chem.* **1974**, *78*, 741.
(33) Vosco, S. H.; Wilk, L.; Nusair, M. *Can. J. Phys.* **1990**, *58*, 1200.
(34) Perdew, J. P. *Phys. Rev. B* **1986**, *33*, 8822.
(35) Becke, A. D. *J. Chem. Phys.* **1993**, *98*, 5648. See also: Becke, A. D. *Phys. Rev. A* **1988**, *38*, 3098.
(36) Clark, T.; Chandrasekhar, J.; Spitznagel, G. W.; Schleyer, P. v. R. *J. Comput. Chem.* **1983**, *4*, 291 and references therein.
(37) Kupka, H.; Cribb, P. H. *J. Chem. Phys.* **1986**, *85*, 1303.
(38) Subbi, J. *Chem. Phys.* **1988**, *122*, 157.
(39) Haarer, D.; Philpott, M. R. In *Spectroscopy and Excitation Dynamics of Condensed Molecular Systems*; Agranovich, V. M., Hochstrasser, R. M., Eds.; North-Holland: New York, 1983; Chapter 2.
(40) Asahi, T.; Matsuo, Y.; Masuhara, H. *Chem. Phys. Lett.* **1996**, *256*, 525.
(41) Assel, M.; Höfer, T.; Laubereau, A.; Keiser, W. *J. Phys. Chem.* **1996**, *100*, 11836.
(42) Craig, D. P.; Petelenz, P. *Chem. Phys. Lett.* **1984**, *105*, 17.
(43) Brovchenko, I. V.; Eilmes, A.; Petelenz, P. *J. Chem. Phys.* **1993**, *98*, 3737.
(44) Petelenz, P.; Slawik, M.; Yokoi, K.; Zgierski, M. Z. *J. Chem. Phys.* **1996**, *105*, 4427 and the references therein.
(45) Frisch, M. J.; Trucks, G. W.; Schlegel, H. B.; Gill, P. M. W.; Johnson, B. G.; Robb, M. A.; Cheeseman, J. R.; Keith, T.; Petersson, G. A.; Montgomery, J. A.; Raghavachari, K.; Al-Laham, M. A.; Zakrzewski, V. G.; Ortiz, J. V.; Foresman, J. B.; Cioslowski, J.; Stefanov, B. B.; Nanayakkara, A.; Challacombe, M.; Peng, C. Y.; Ayala, P. Y.; Chen, W.; Wong, M. W.; Andres, J. L.; Replogle, E. S.; Gomperts, R.; Martin, R. L.; Fox, D. J.; Binkley, J. S.; Defrees, D. J.; Baker, J.; Stewart, J. P.; Head-Gordon, M.; Gonzales, C.; Pople, J. A. *GAUSSIAN 94*, revision E.1; Gaussian, Inc.: Pittsburgh, 1995.
(46) *Dmol*, *InsightII*, release 95.0; Biosym/MSI: San Diego, 1995.
(47) Andruniow, T.; Pawlikowski, M. *Chem. Phys. Lett.*, in press.
(48) Zgierski, M. Z. *Chem. Phys.* **1986**, *108*, 61.
(49) Kadama, K.; Baundrauk, A. D. *Chem. Phys. Lett.* **1981**, *80*, 248.
(50) Penner, A.; Siebrand, W. *Chem. Phys. Lett.* **1976**, *39*, 11.